

Verifying InSAR Derived Vertical Differential Displacements by Leveling – Application along the Mornos Open Aqueduct

Ioannis KOTSIS, Spyros KARAMITSO, Charis KONTOES, Demetris PARADISSIS, Olga SYCIOTI, Panagiotis ELIAS, Greece and Pierre BRIOLE, France

Key words: Crustal Displacements, InSAR, Interferometry, Leveling

SUMMARY

In this project, a method to extract tectonic activity – induced vertical displacements from InSAR along one-dimensional features (roads, pipelines, aqueducts), is presented and the reliability of this method is evaluated. The evaluation is performed by a comparison of InSAR results and terrestrial surveying. The test field is in the north – west region of Attiki prefecture, 20km from the center of Athens and the one – dimensional feature is the Mornos aqueduct. The displacements – at least the greatest part – are due to the 07/09/1999 Athens earthquake.

The way to make InSAR and terrestrial surveying data compatible and therefore directly comparable includes the well-known InSAR processing actions of interferogram filtering for partial noise removal and phase unwrapping to resolve the $\text{mod}_{2\pi}\Phi$ ambiguity. It also includes geodetic reference system transformations – necessary in the cases when the interferogram is in other reference system than the one used in terrestrial measurements, and computation of incidence angles for every interferogram target to convert LOS projected displacements to vertical ones. Ultimately, the problem of temporal decorrelation is dealt with mathematical modeling of the displacement field.

It is finally concluded that InSAR interferograms, after appropriate processing, are indeed capable of providing sufficiently accurate and reliable vertical differential displacement data.

Verifying InSAR Derived Vertical Differential Displacements by Leveling. Application along the Mornos Open Aqueduct

Ioannis KOTSIS, Spyros KARAMITSO, Charis KONTOES, Demetris PARADISSIS, Olga SYCIOTI, Panagiotis ELIAS, Greece and Pierre BRIOLE, France

1. BACKGROUND

The 07/09/1999, 11^h 56^m 50^s UTC, Mw = 5.9 Athens earthquake, was one of the most significant natural disasters that struck Greece in the 20th century. This earthquake claimed the lives of 143 people, caused the severe injury of many others and was responsible for the collapse of several buildings mainly in the northwestern suburbs region of the Greek capital, and rendered useless many others. The approximate location of the epicenter of the earthquake was 38.10°N, 23.56°E, roughly 20km from the center of Athens.

The vertical displacements of the Earth's surface caused by this major tectonic event, were investigated by the Institute of Space Applications and Remote Sensing of National Observatory of Athens (NOA/ISARS) in cooperation with the Higher Geodesy Laboratory of the National Technical University of Athens, (NTUA/HG) and the Institut de Physique du Globe, Paris (IPGP), with space born Synthetic Aperture Radar Interferometry (InSAR), using ERS – 2 data. This project was completed a few months after the earthquake. InSAR processing revealed maximum LOS projected surface subsidence of approximately 9cm. The region where the maximum of deformation occurs roughly coincides with the main shock epicenter, being approximately 3km away (Kontoes et al, 2000).

This region is very close to Mornos open aqueduct, used for the water supply of Athens. Although the aqueduct was not damaged, it would be a good test structure to investigate the vertical displacement with leveling as well, since leveling data, before the earthquake existed. The distance of this part of the aqueduct from the epicenter is less than 2.5km (Papanastassiou D. et al, 1999).

A leveling project on the aqueduct was initiated by NTUA/HG which lasted two months (March – April 2001). The earlier data had been taken in 1984. No leveling data were available for the time interval 1984-2001, so the non seismic deformation is not accounted for. However, no major seismic event took place in that time interval as well.

The interferogram, as derived by the InSAR processing work, the leveling path legs, and the longitudinal axis of the open aqueduct, are presented in the figure 1.

In later sections, the InSAR processing and the terrestrial surveying will be presented with more detail.

The primary objectives of this work are to validate the products of SAR Interferometry as applied for the mapping of a vertical displacement field of an earthquake.

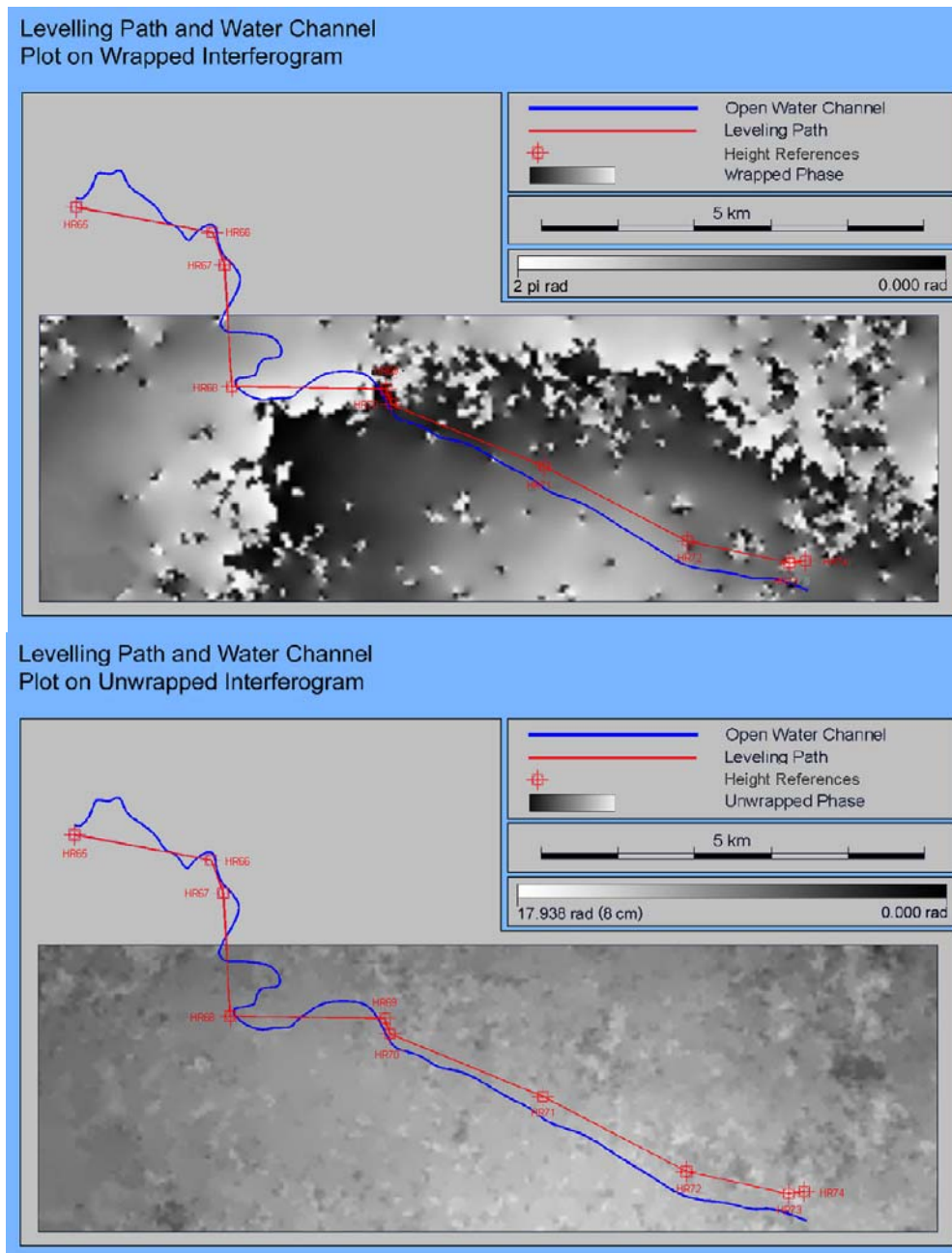


Figure 1: Leveling Path Legs Plot and aqueduct Plot on wrapped (up) and unwrapped (down) interferogram. Unfortunately, a significant part of the leveling, in particular the legs HR65 – HR66, HR66 – HR67 and HR67 – HR68, do not have interferogram correspondence. (For clarity purposes, only the segments connecting the high references are displayed. The actual leveling path follows the channel)

2. INSAR PROCESSING

Many images were acquired and processed to detect and measure the earthquake – induced deformation field. Using CNES DIAPASON InSAR processing software, eight interferograms were produced, from which for this particular work only the four co – seismic were of interest. From these four interferograms, one particular was selected for this project, mainly because of the clarity of the deformation phase signal. This interferogram is identified by the data of the image combination as shown in table 1 below:

Image	Orbit #	Acquisition Date/Time	Frame #	Track #	Altitude of Ambiguity h_a
Master	17854	19/09/1998 09:06:51 UTC	2835	465	-67.236 m
Slave	23365	09/10/1999 09:06:47 UTC	2835	465	

Table 1: Interferogram SAR image combination data.

The influence of the terrain relief on the interferogram was lifted using a Digital Elevation Model with grid size 50m x 50m, with an estimated standard height deviation of approximately 10m.

Apart from the interferometric processing, a fault modeling procedure produced a simulated synthetic interferogram taking as input the parameters of the fault and the magnitude of the shock. The interferogram produced by the InSAR processing, as well as the modeled one, are presented in figure 2.

The area of interest is located at the northwest part of the interferogram, where the leveling work was done, part of which is not covered by the interferogram due to absence of Digital Elevation Model coverage. This area is presented out in figure 2 as solid black.

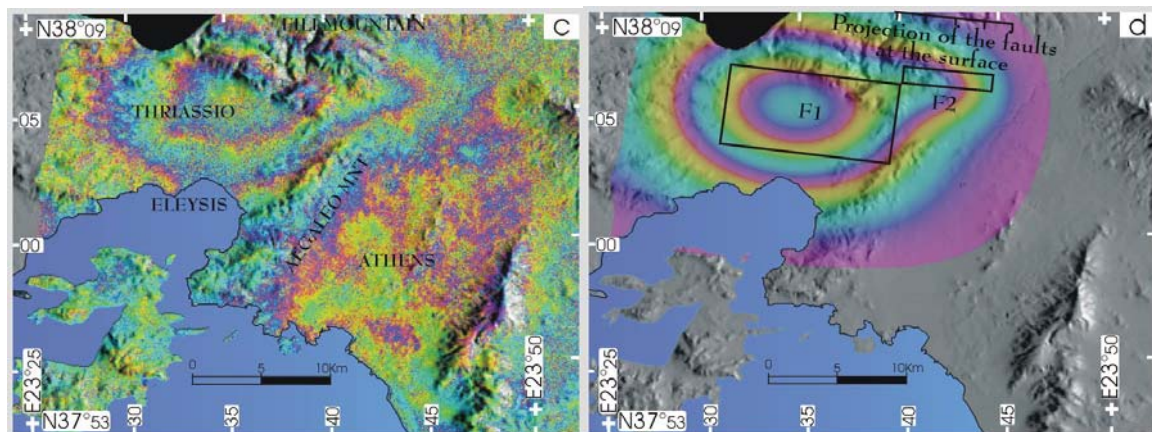


Figure 2: InSAR processing output interferogram (left) and the simulated interferogram (right). Solid Black colored area in NW has no interferogram coverage due to lack of DTM data (Kontoes et al, 2000).

3. TERRESTRIAL SURVEYING

The first leveling work on the aqueduct was done in 1984, covering its whole length of approximately 200km. A special trigonometric leveling technique was used which had been developed at the Higher and Satellite Geodesy Laboratory, giving the same level of accuracy as conventional leveling but being a lot faster, (Balodimos, 1979). The accuracy of the work was estimated to be in the order of a few mm from height reference to height reference. After the earthquake and much InSAR processing it became apparent that the aqueduct was crossing fringes which were indicating vertical displacements. A standard leveling project was necessary to evaluate the InSAR results and it took place in 2001. The distance covered was 40km (two - way) with similar accuracy to the previous work. The same height references were used as well. Table 2 shows the height differences between 1984 and 2001.

Height reference	Height differences between 2001 – 1984 (m)
HR65-HR66	-0.008
HR66-HR67	-0.003
HR67-HR68	-0.021
HR68-HR69	-0.004
HR69-HR70	-0.005
HR70-HR71	-0.003
HR71-HR72	-0.001
HR72-HR73	-0.003
HR73-HR74	-0.001

Table 2: Height differences between 2001 and 1984, obtained by leveling and height triangulation respectively.

4. RENDERING INSAR DATA COMPATIBLE TO LEVELING

The differential displacement data derived by the two different techniques are incompatible and consequently a direct comparison. These incompatibilities specifically are the following:

- InSAR processing provides wrapped interferograms, which means that not the full phase difference Φ is provided, but only its fractional part $\text{mod}_{2\pi}\Phi$.
- InSAR does not provide the true vertical differential deformations, but their projection on the line of sight (LOS).
- In this particular case, the reference systems of the leveling and the InSAR processing and outcome work are different. In particular, InSAR interferograms are on ED 50 UTM 34, while the total of the leveling work was completed with respect to mean sea level and the height references positions were registered to Hellenic Geodetic Reference Systems 87 (HGRS 87).

- The interferograms are corrupted by noise, which – mainly due to temporal decorrelation - may reach extremely high levels (perhaps even 1π), a fact that is a potential danger for the reliability of the point - wise displacement extraction.

In the sections, the procedure used to lift the incompatibilities is presented.

5. WRAPPED INTERFEROGRAM FILTERING

The wrapped interferogram part, corresponding to the defined area of interest, underwent a simple filtering procedure. The primary objective of this action was to minimize the odds of the incoming phase unwrapping failure, while a secondary purpose was the improvement of the wrapped and unwrapped interferogram appearance, to make qualitative evaluations as effortless as possible.

The filter used, was simple 2D space median filter, applied on both the real ($\cos(\psi_{i,j})$) and imaginary ($\sin(\psi_{i,j})$) parts of a virtual unitary magnitude signal $e^{j\psi_{i,j}} = \cos(\psi_{i,j}) + j\sin(\psi_{i,j})$ whose phases were those of the input un – filtered interferogram ($\psi_{i,j}$). In other words, the 2D space filter was applied on a unitary signal to which the phases of the input interferogram were projected. The phases $\psi_{flv,i,j}$ comprising the filtered interferogram, were extracted through an arc tan() operation by the filtered real and imaginary parts of the virtual signal. The filtering procedure is best defined by the following formula:

$$\psi_{flv,i,j} = \arctan \left(\frac{\sum_{j=j_0-\frac{k-1}{2}}^{j_0+\frac{k-1}{2}} \sum_{i=i_0-\frac{k-1}{2}}^{i_0+\frac{k-1}{2}} \cos(\psi_{i,j})}{k^2}, \frac{\sum_{j=j_0-\frac{k-1}{2}}^{j_0+\frac{k-1}{2}} \sum_{i=i_0-\frac{k-1}{2}}^{i_0+\frac{k-1}{2}} \sin(\psi_{i,j})}{k^2} \right)$$

In figure 3, the different steps of interferogram filtering procedure are shown.

6. PHASE UNWRAPPING

In order to achieve a reliable comparison of the differential vertical displacement as provided by SAR interferometry and leveling, the integer phase ambiguous nature of SAR interferograms had to be lifted. Towards that end, various 2D phase unwrapping techniques (Quality Guided Path Following, Unweighted Least Squaring, Weighted Least Squaring and Minimum LP Norm) were implemented and their outcomes were comparatively evaluated. The unwrapped interferograms produced by the several techniques applied on the initial wrapped interferogram, were evaluated mainly in terms of minimum discontinuity criteria.

As a result, it was determined that the most effective technique – in this particular case – was the weighted least squaring. The phase observations weights for the weighted least squaring were obtained by the cross – correlation (coherence) values computed by DIAPASON InSAR processing software as output of the relative geometry parameter computation between master and slave SAR images. The input wrapped interferogram and coherence image and the output unwrapped interferogram are shown in figure 4.

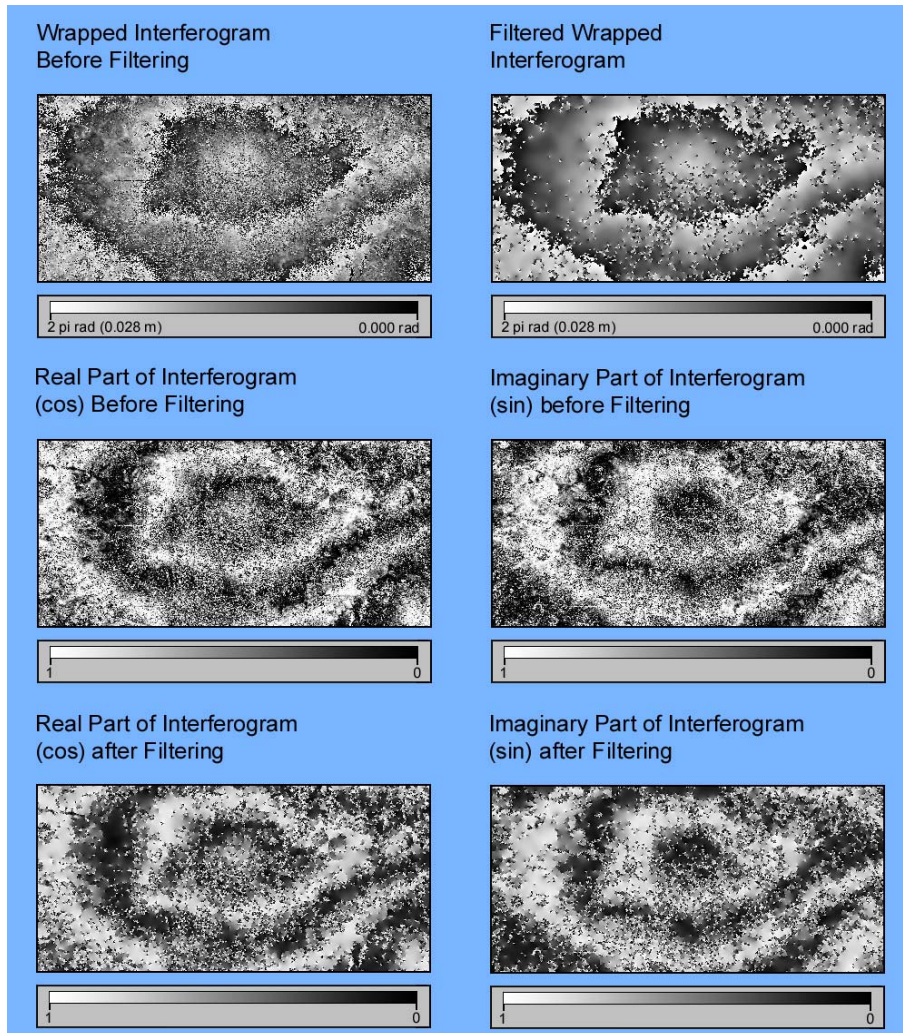


Figure 3: Different Interferogram Filtering Processing Stages.

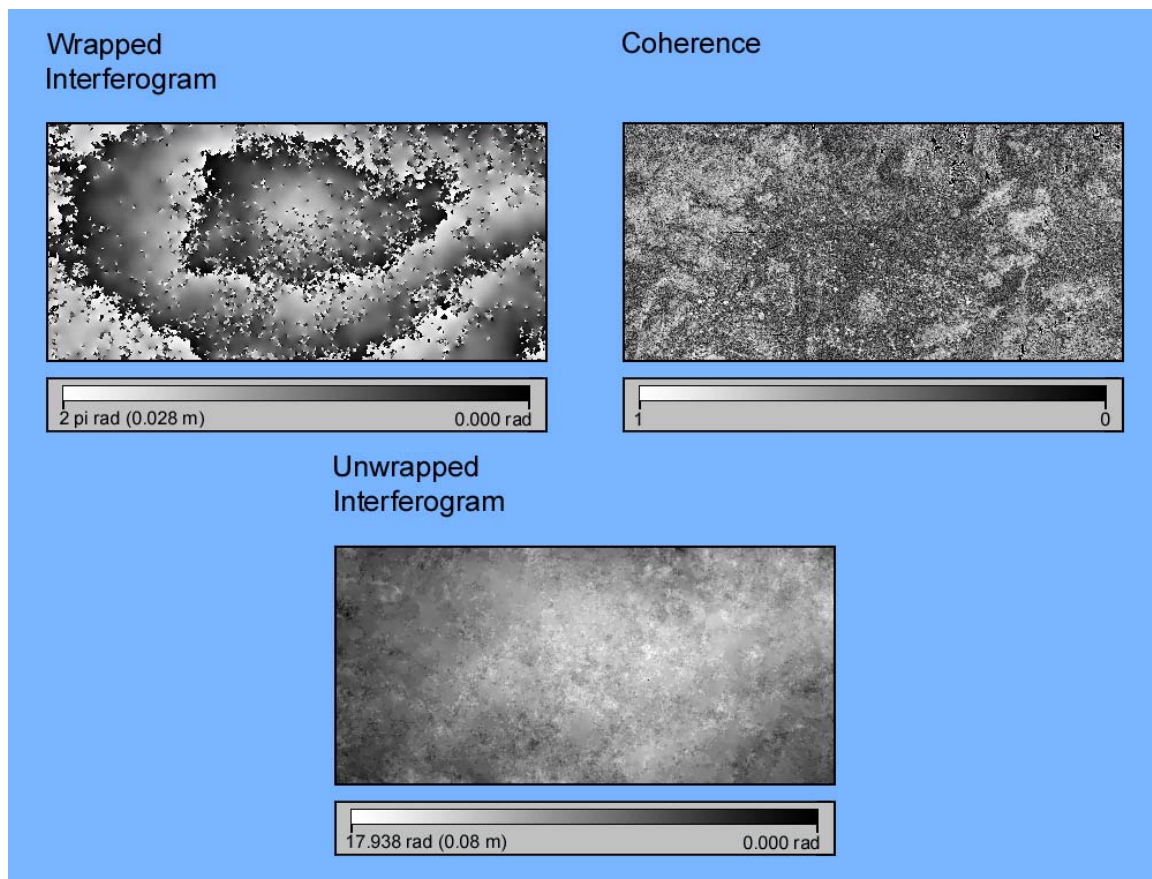


Figure 4: Phase Unwrapping: The input wrapped interferogram (up left), the coherence image used to obtain weighting data for the least squaring unwrapping process (up right) and the output unwrapped interferogram (down).

7. GEODETIC REFERENCE SYSTEM CONVERSION

A geodetic reference system incompatibility issue had to be resolved: The ortho geometry unwrapped interferogram was provided by CNES DIAPASON InSAR processing software at the same geodetic reference system the Digital Elevation Model was, that is UTM map projection zone 34, on ED 50 Euro Mean Datum (using Hayford Ellipsoid). The coordinates of the height references were expressed however, in HGRS 87 (Hellenic Geodetic Reference System 1987), using Transverse Mercator Map projection with a zero meridian at 24° .

To overcome this geodetic reference system incompatibility, the initial ED 50 UTM 34 interferogram was resampled a HGRS 87. This procedure comprised the following steps applied for every single pixel of the interferogram, maintaining through every step the unwrapped phase of the interferogram:

- Conversion of the ED 50 UTM map coordinates (eastings and northings – e, n) to ED 50 ellipsoidal coordinates (latitude and longitude – φ , λ), assigning at the same time each

- target pixel' s orthometric heights (H) from the DTM used in the interferometric processing.
- Conversion of the orthometric heights into geometric (h), implementing a constant additive geoid undulation value (N) for the entire area of interest, exploiting the fact that the geoid in this area is relatively “flat”, in other words exhibits a very low gradient. This value was "obtained" by the Ohio State University OSU 91 Geoid Model, and re - computed for ED 50.
 - The ED 50 ellipsoidal coordinates were converted to ED 50 Cartesian coordinates (X, Y, Z).
 - The ED 50 geocentric Cartesian coordinates were converted to HGRS 87 geocentric Cartesian coordinates, assuming only a parallel shift.
 - The HGRS 87 geocentric Cartesian coordinates were converted to HGRS 87 ellipsoidal (latitude and longitude – φ, λ) coordinates. At this point the height information of every point was discarded.
 - Ultimately, the HGRS 87 ellipsoidal (latitude and longitude – φ, λ) coordinates were converted to HGRS 87 Transverse Mercator projection coordinates (eastings and northings – e, n).

8. LINE OF SIGHT CORRECTION

Even following the geodetic reference system incompatibility lifting, a comparison is not possible because the HGRS 87 unwrapped interferogram, provides the differential vertical displacements for each target pixel as projected on the LOS vector ($\Phi_{\text{LOS}}(e, n)$) of the particular target, and not the vertical differential displacement themselves ($\Phi_{\text{du}}(e, n)$), as is the case in leveling:

$$\Phi_{\text{LOS}}(e, n) = \cos(\text{In}(e, n))\Phi_{\text{du}}$$

In order to determine the differential vertical displacements from their LOS projection, the values of incidence angle ($\text{In}(e, n)$) for each target pixel are required. The incidence angle computation procedure is based on satellite trajectory data and the position of the target.

Initially, for every target the zero - Doppler position of the space born SAR sensor had to be computed. This was achieved through the following process, preferably for the “master” (or “reference”) image.

Third degree polynomials were fitted with least squares to the known satellite position vectors $\vec{r}(t)$ as derived by ERS – 1/2 operational orbits and provided at every SAR image header file. These polynomials simply provide satellite position vectors in the orbit's terrestrial geocentric reference frame as functions of time. Three polynomials were derived, one for every ordinate X, Y and Z. Three equations are obtained.

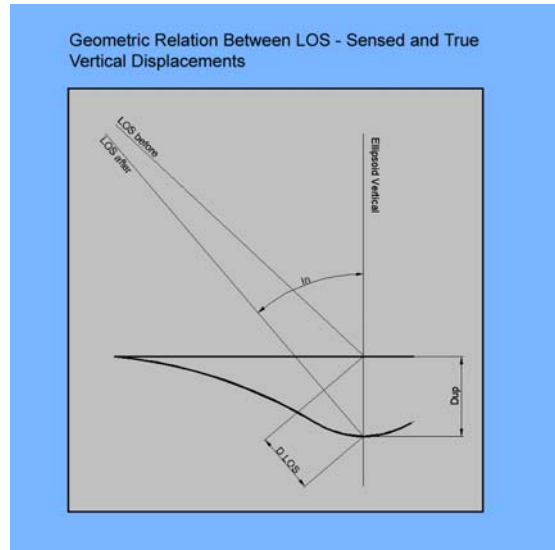


Figure 5: Relative Geometry of true vertical deformation and deformation provided by InSAR.

Exactly the same procedure was applied for the satellite velocity vectors $\vec{r}(t)$. Three more equations are obtained.

For every single target the following procedure is performed:

- The map projection coordinates of the target are converted to geocentric cartesian coordinates in the geodetic terrestrial reference frame in which the satellite orbits are provided (in this particular case from HGRS 87 map coordinates to ITRF 96 geocentric Cartesian coordinates).
- The mean Doppler frequency shift is computed by CNES DIAPASON software at the early stages of processing, and without significant error is assumed to hold for every pixel target. Doppler frequency shift is expressed as function of satellite position and velocity vectors and target position by the following equation:

$$f(i, j) = \frac{2(\vec{r}(i, j) - \vec{r}(t_1)) \cdot \vec{r}(t_1)}{\lambda \left(\left| \vec{r}(i, j) - \vec{r}(t_1) \right| \right)}$$

- A total of seven equations have been so far accumulated, and equal number of unknowns has been introduced, three for satellite position vector, another three for satellite velocity vector and one more for the particular time. A non – linear seven-equation system is comprised for the estimation of seven unknowns. The system is linearized with Taylor series expansion, and solved iteratively. The solution of the aforementioned system provides deliberately the estimation for satellites position state vector, while the estimations of velocity and time appear as by – products.

- Knowing satellite and target position vectors, the unitary line – of – sight vector can be calculated simply as stated by the following vector equation below:

$$- \quad \text{LOS}(i, j) = \frac{(\vec{r}(i, j) - \vec{r}(t_1))}{|\vec{r}(i, j) - \vec{r}(t_1)|}$$

- The target position ellipsoidal coordinates (latitude, longitude) are calculated, expressed on the same geodetic terrestrial frame used to express the orbits and the target coordinates in the previous step of this procedure.
- With the target's latitude and longitude $(\varphi_{i,j}, \lambda_{i,j})$, the LOS vector components are transformed into local geodetic reference system (delta north – Dn, delta east – De, delta up – Du) by means of a rotation matrix. This is expressed by the equation below:

$$- \quad \begin{bmatrix} \text{DX}(t) \\ \text{DY}(t) \\ \text{DZ}(t) \end{bmatrix} \text{R}(\varphi_{i,j}, \lambda_{i,j}) = \begin{bmatrix} \text{Dn}(t) \\ \text{De}(t) \\ \text{Du}(t) \end{bmatrix}$$

- Essentially, the third component of the LOS vector as expressed in a local geodetic reference system is actually the direction cosine for the “up” axis of the system, and consequently, the cosine of incidence angle In . Thus the incidence angle can be derived through a simple arc tan operation: $\text{In} = \arctan(\text{Du})$

9. DIFFERENTIAL VERTICAL DISPLACEMENT SMOOTHING

Thorough and careful examination of the unwrapped interferogram, reveals the presence of “local” phase anomalies in some areas extending from one to several pixels, whose phase is very far from the prevailing values in the surrounding region. These anomalies have survived the filtering procedure described previously.

It is beyond the scope of this particular project to explore and study the cause of such phase “residuals”, but it could be assumed that they stem from local tropospheric spatial differentiations, or other forms of temporal decorrelation. Regardless of their cause at all, they cannot be attributed to the tectonic activity of Athens earthquake. Additionally, it was observed that the areas infected by these anomalies, present significantly low correlation, as observed in the coherence images and therefore, they must be excluded from this analysis.

It was decided that the exclusion of these phase anomalies, in other words the smoothing of the interferogram phases, should be performed by exploiting the low phase gradient of the tectonic deformations, by fitting with weighted least squares a 3D mathematical surface model to the unwrapped, LOS corrected interferogram phases $\Phi_{\text{du}}(e, n)$. This surface would provide the vertical deformation for each pixel target given its map coordinates e, n as input.

In order to insure minimized constraints for the pattern of the displacement field, the most general form of m - th degree 3D surface mathematical model was used:

$$\begin{aligned} \Phi_{du}(e, n) = & -(a_0 + a_{e1} \cdot e^1 + a_{e2} \cdot e^2 + a_{e3} \cdot e^3 + \dots + a_{em} \cdot e^m + \\ & + a_{n1} \cdot n^1 + a_{n2} \cdot n^2 + a_{n3} \cdot n^3 + \dots + a_{nm} \cdot n^m + a_{en} \cdot e^1 \cdot n^1 + \\ & + a_{e1n(m-1)} \cdot e^1 \cdot n^{(m-1)} + a_{e2n(m-2)} \cdot e^2 \cdot n^{(m-2)} + \dots + a_{e(m-2)n2} \cdot e^{(m-2)} \cdot n^2 + a_{e(n-1)n1} \cdot e^{(m-1)} \cdot n^1) \end{aligned}$$

After several runs, it was determined that a degree a surface polynomial degree higher than third, would be redundant, since it was not offering no improvement in terms of a posteriori variance and measurement residuals. All higher degree coefficients were essentially zero. The produced surface is presented in figure 6 with two different ways of visualization, color map and contour plots.

10. ESTIMATION AND COMPARISON OF INSAR AND LEVELING VERTICAL DIFFERENTIAL DISPLACEMENTS

Using the 3D surface model derived in the previous section, it is possible to extract from it a profile section of the vertical differential displacements as provided by InSAR, along the leveling traverse. One of the advantages of mathematical modeling for the differential displacements is the using extrapolation, making it possible to obtain displacement estimations in areas not covered by the interferogram. This was very useful in this project, since a significant part of the leveling, falls out of the interferogram.

Using the model derived previously, the vertical differential deformation is estimated at the height reference positions. Thus the vertical differential displacement profile section as provided by InSAR along the leveling path legs is computed as follows:

$$[D_{HR_x}, \Phi_{du}(e_{HR_x}, n_{HR_x})]$$

$D_{HR_{i,j}}$ stands for the total sum of horizontal distances between successive legs of the leveling up $HR_{i,j}$ point. Since differential vertical displacements are the issue, an origin has to be defined, and this was decided to be HR 65. Consequently, its displacement is set to zero. All other vertical displacements are provided with respect to HR65. Profile data for InSAR and leveling are presented in Table 3, and the graphs are presented in figure 7.

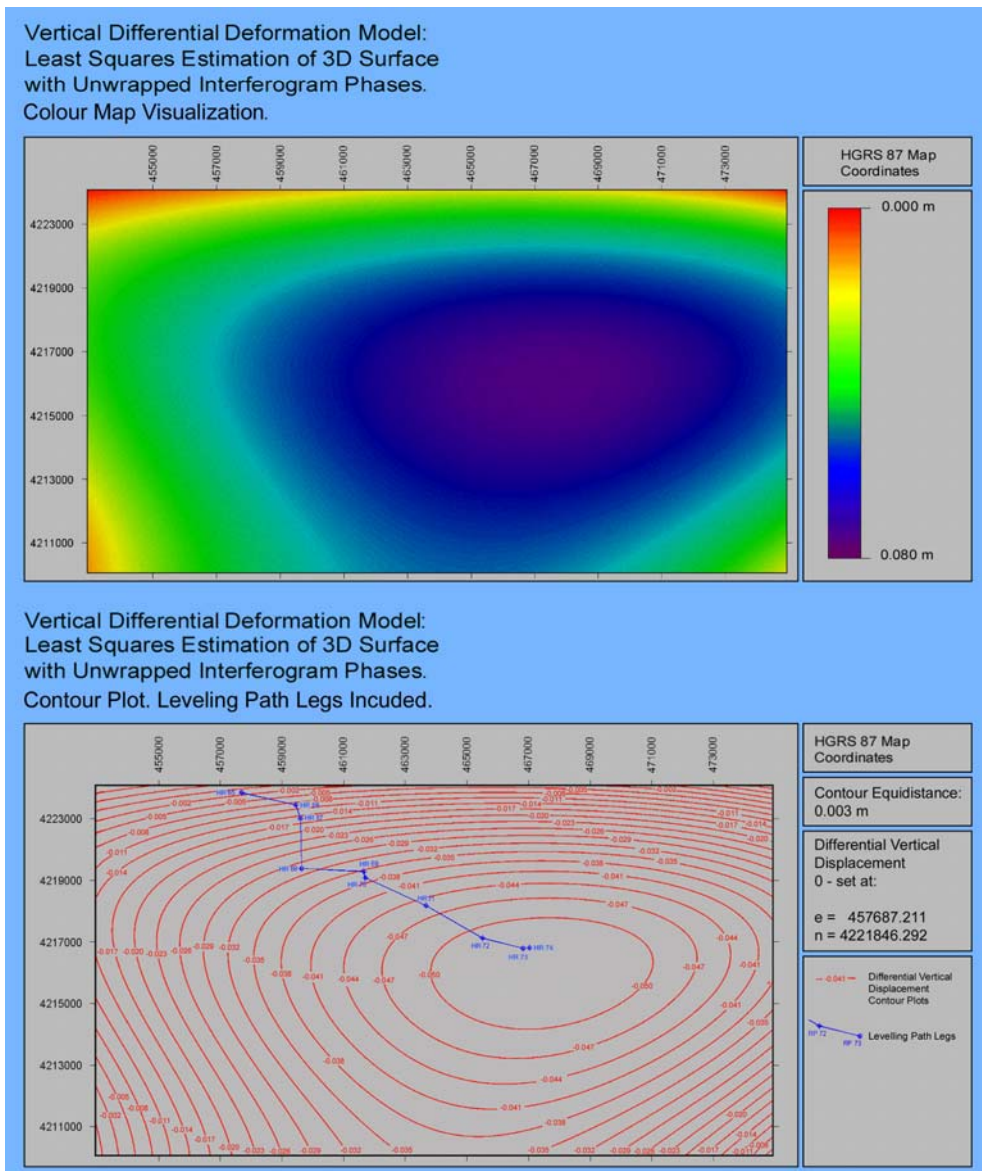


Figure 6: Differential Vertical Displacement Modeling by means of 3D third degree mathematical surface. Visualization with color (up) and contour plot (down).

11. CONCLUSIONS

In general terms, by studying the profiles above (fig. 6), it can be concluded that no major discrepancies occur between the differential vertical displacements as obtained by InSAR and leveling.

- Both exhibit the same trend (same signs of vertical displacement for all legs between the two profiles), from HR 65 to HR 74.

- There also appears to be an agreement between the two profiles in whatever has to do with respect the gradient of the vertical displacement and there is no evidence of any systematic deviation between them.
- The vertical displacement differences between the two profiles do not exceed 6mm. These differences are due to the trigonometric leveling errors, in 1984 to the leveling errors in 2001, to InSAR interferogram noise, to the interferogram digital terrain model induced errors (the altitude of ambiguity of about -67 m and the DTM standard deviation accounts for 0.15 phase cycles) and to some.

The final conclusion from this whole work is that indeed InSAR provides displacements with an accuracy of a few mm.

Height Reference	Reper Position HGRS 87 Map Coordinates		Horizontal Distance between successive height reference (m)	Leveling Path Leg Horizontal Distance Sum (m)	Differential Vertical Displacements with respect to HR65 (m)		Differential Vertical Displacement Differences (Leveling – InSAR) (m)
	e (m)	n (m)			D Hz	Σ D Hz	
HR 65	457687.211	4221846.292	0.000	0.000	0.0000	0.0000	0.0000
HR 66	459452.656	4221448.342	1809.740	1809.740	-0.0080	-0.0085	0.0005
HR 67	459596.995	4221007.964	463.429	2273.169	-0.0110	-0.0150	0.0040
HR 68	459637.956	4219382.052	1626.428	3899.597	-0.0320	-0.0300	-0.0020
HR 69	461650.111	4219285.583	2014.466	5914.064	-0.0360	-0.0350	-0.0010
HR 70	461704.263	4219080.368	212.240	6126.303	-0.0410	-0.0370	-0.0040
HR 71	463673.404	4218179.781	2165.311	8291.614	-0.0440	-0.0450	0.0010
HR 72	465504.885	4217124.455	2113.773	10405.387	-0.0450	-0.0510	0.0060
HP 73	466827.810	4216790.128	1364.516	11769.904	-0.0480	-0.0530	0.0050
HR 74	467031.711	4216809.064	204.778	11974.682	-0.0490	-0.0530	0.0040

Table 3: Vertical Differential Deformation along leveling path and path differences, as obtained by SAR Interferometry and conventional leveling data.

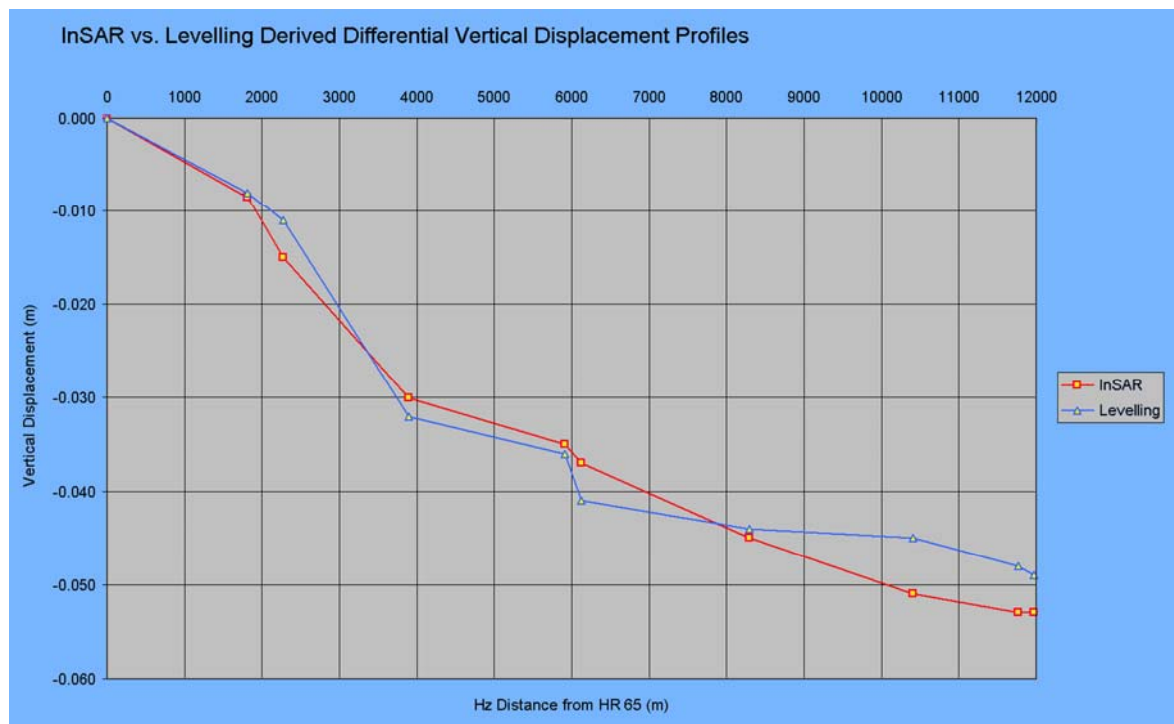


Figure 7: Vertical Differential Deformation Profile Sections as obtained by SAR Interferometry and conventional leveling.

REFERENCES

- Balodimos D. (1979) The development of a special trigonometric leveling technique, *Tecnika chronica* Vol. 3, Athens, (in Greek).
- Deltsidis P., Saridakis M. (2001) Displacement determination with terrestrial and satellite methods, Diploma Thesis, Dionysos Satellite Observatory, National Technical University of Athens, (in Greek).
- Kontoes C., Elias P., Sykioti O., Briole P., Remy D., Sachpazi M., Veis G., Kotsis I. (2000) Displacement Field Mapping and Fault Modeling of the Mw = 5.9, September 7, 1999 Athens Earthquake based on ERS – 2 Satellite RADAR Interferometry, *Geophysical Research Letters*, Vol. 27, No 24, 3989-3992.
- Liu G., Chen Y., Ding X., Li Z. (2002) Monitoring Ground Settlement in Hong Kong with Satellite SAR Interferometry, FIG XXII International Congress Washington D.C., USA.
- Odiijk D., Kenselaar F., Hanssen R. (2003) Interaction of Leveling and InSAR Data For Land Subsidence Monitoring, 11th International FIG Symposium Santorini, Greece.
- Papanastassiou D., Stavrakakis G. Drakatos G. and Papadopoulos G. (1999) The Athens, September 7, 1999, $M_s=5.9$, Earthquake: First Results on the Focal Properties of the Main Shock and the Aftershock Sequence, *Ann. Geol. des Pays Helleniq*”, submitted for publication.

Technical Report (1984) Mornos Aqueduct Leveling, Higher Geodesy Laboratory, National Technical University of Athens.

BIOGRAPHICAL NOTES

Mr. Ioannis Kotsis, Surveying Engineer, is a Ph.D. candidate in Higher and Satellite Geodesy Laboratory of School of Surveying of National Technical University of Athens, and works as technical consultant in TopoMet S.A.

Address: Iroon Polytexneiou 9, 15780, Zografou, Greece, Tel.: +302107722667, email: jkotsis@survey.ntua.gr

Mr. Spiros Karamitsos, Surveying Engineer, is a Ph.D. candidate in Higher and Satellite Geodesy Laboratory of School of Surveying of National Technical University of Athens, and works for the Ministry of Environment and Public Works.

Address: Iroon Polytexneiou 9, 15780, Zografou, Greece, Tel. +302107722667, email: karamits@central.ntua.gr

Dr. Harris Kontoes, Surveying Engineer, is a researcher in the Institute of Space Applications and Remote Sensing of the National Observatory of Athens.

Address: Vas. Pavlou and Metaxa Str., 15236, Palaia Penteli, Greece. Tel.: +302108109186, email: kontoes@space.noa.gr

Prof. Demetris Paradissis, Surveying Engineer, is a Professor in the Higher and Satellite Geodesy Laboratory of School of Surveying of National Technical University of Athens.

Address: Iroon Polytexneiou 9, 15780, Zografou, Greece, Tel.: +302107722666, email: dempar@central.ntua.gr

Dr. Olga Sykioti, Geologist, is a research assistant in the Institute of Space Applications and Remote Sensing of the National Observatory of Athens.

Address: Vas. Pavlou and Metaxa Str., 15236, Palaia Penteli, Greece. Tel. +302108109195, email: sykioti@space.noa.gr

Mr. Panagiotis Elias, Electronics Engineer, is a research and technical assistant in the Institute of Space Applications and Remote Sensing of the National Observatory of Athens.

Address: Vas. Pavlou and Metaxa Str., 15236, Palaia Penteli, Greece. Tel.: +302108109186, email: pelias@space.noa.gr

Dr. Pierre Briole, Geophysicist, is a researcher in Departement de Sismologie, Institut de Physique du Globe de Paris. Address: 4 Place Jussieu - 75005 Paris, tel : (33 1) 44 27 48 93 fax: (33 1) 44 27 38 94, email: briole@ipgp.jussieu.fr

CONTACTS

Mr. Ioannis Kotsis

National Technical University of Athens / Dionysos Satellite Observatory

9 Iroon Polytechniou, 15780, Zographou

Athens

Hellas

GREECE

Tel. + 30 210 772 2667

Fax + 30210 772 2670

Email: jkotsis@survey.ntua.gr

Web site: <http://www.survey.ntua.gr/main/labs/hgeod/hgeod-g.html>